Electric Power Systems Research 154 (2018) 276–286

Contents lists available at ScienceDirect

Electric Power Systems Research

journal homepage: www.elsevier.com/locate/epsr

Real-time co-simulation of adjustable-speed pumped storage hydro for transient stability analysis

Manish Mohanpurkar[a,*], Abdelhamid Ouroua[b], Rob Hovsapian[a], Yusheng Luo[a], Mohit Singh[c], Eduard Muljadi[d], Vahan Gevorgian[d], Peter Donalek[e]

[a] Idaho National Laboratory, Idaho Falls, ID 83415, USA
[b] Center for Electromechanics, University of Texas, Austin, TX 78758, USA
[c] Commonwealth Edison, Chicago, IL, Illinois
[d] National Renewable Energy Laboratory, Golden, CO 80401, USA
[e] MWH-Stantec, Chicago, IL, USA

ARTICLE INFO

Article history:
Received 29 March 2017
Received in revised form 31 July 2017
Accepted 9 August 2017

Keywords:
Adjustable speed
Doubly-fed induction machine
Digital real-time simulator (DRTS)
Real-time simulation
Power systems
Transients
Co-simulation
Hydrodynamics
Hydroelectric power generation
Power system stability

ABSTRACT

Pumped storage hydro (PSH) based generation of electricity is a proven grid level storage technique. A new configuration i.e., adjustable speed PSH (AS-PSH) power plant is modeled and discussed in this paper. Hydrodynamic models are created using partial differential equations and the governor topology adopted from an existing, operational AS-PSH unit. Physics-based simulation of both hydrodynamics and power system dynamics has been studied individually in the past. This paper demonstrates a co-simulation of an AS-PSH unit between penstock hydrodynamics and power system events in a real-time environment. Co-simulation provides an insight into the dynamic and transient operation of AS-PSH connected to a bulk power system network. The two modes of AS-PSH operation presented in this paper are turbine and pump modes. A general philosophy of operating in turbine mode is prevalent in the field when the prices of electricity are high and in the pumping mode when prices are low. However, recently there is renewed interest in operating PSH to also provide ancillary services. A real-time co-simulation at sub-second regime of AS-PSH connected to the IEEE 14 bus test system is performed using digital real-time simulator and the results are discussed.

1. Introduction

Electric grids around the world are undergoing a progressive transition towards a more modernized, resilient, and self-governing architecture and operation. All three – generation, transmission, and distribution sectors are experiencing significant improvements and upgrades in terms of infrastructure development, increased penetrations by variable renewable generation, and novel management techniques. The generation sector of the future may be well characterized as a unique blend of conventional resources and non-conventional, non-dispatchable variable output resources. The optimum combination of generation resources is based on their capability to complement one another, and to supply real-time daily evolving demand according to established reliability criteria. The transmission sector is rapidly evolving with infrastructure upgrades of transmission line design and operation including extra high voltage alternating and direct current transmission lines, multi-phase designs, hi-fidelity measurement systems such as phasor measurement units, localized real-time capacity monitoring, dynamic line rating, high speed communications, and, deployment of flexible AC transmission devices (FACTS). In the context of deregulation, the Federal Energy Regulatory Commission (FERC) issued Order no. 888 that requires utilities to provide fair open-access of transmission resources to all market participants led a significant transformation [1]. The distribution sectors are adopting innovative concepts such as microgrids, distributed energy resources, reconfigurability and self-healing network.

Wide-band semiconductor based power electronic converters and their applications have a potential to provide a greater flexibility in all these three sectors of the grid. Prior to deregulation, power generation plants in bulk power electric grids were deterministic and dispatchable; hence they are predictable. However, the current and future trend of increasing penetration levels of wind and solar photovoltaic installations on the grid impart non-trivial stochas-

* Corresponding author.
E-mail addresses: a.ouroua@cem.utexas.edu (A. Ouroua), Mohit.Singh@comed.com (M. Singh), Eduard.Muljadi@nrel.gov (E. Muljadi), P.Donalek@ieee.org (P. Donalek).

http://dx.doi.org/10.1016/j.epsr.2017.08.010

Variable interpretation

x	location variable (m)
t	time variable (s)
U	flow velocity in (m/s)
H	head of the flow (m)
a	pressure wave velocity (m/s)
g	gravitational acceleration
D	internal diameter of pipe (m)
f	frictional factor
h	height (m)
k_{fp}	normalized friction coefficient
$\bar{h}$	height (m)
$\bar{P_m}$	mechanical power (p.u.)
A_t, D_{turb}	turbine specific constants
$\bar{\omega}$	angular velocity (rads/s)
α	constants for simplification
C_1, C_2, C_3, C_4, C_5	boundary level constants (p.u.)
$T_{(s)}$	hydraulic circuit transfer function
$\bar{h}_{num}$	per unitized head values
$\bar{u}_{num}$	per unitized flow values
T	time constant of hydro channel
Z	impedance of hydro channel
$i_{(ra)}$, $i_{(rb)}$, $i_{(rc)}$	rotor circuit currents in 3 phases
$i_{(rd)}$	direct axis rotor circuit current
$i_{(rq)}$	quadrature axis rotor circuit current
ψ	phase difference
P_{total}	total electrical power generated
P_{ms}, P_{mr}	stator and rotor power
$slip$	slip of the induction machine

ticity to the generation dispatch [2]. The renewable energy sources are connected in both aggregated and standalone configurations, thus, diversifying the portfolio. The increase in renewable energy sources coupled with the retiring of thermal power plants is leading to reduced inertia in the grid [3].

System operators and utilities need adequate flexible resources such as hydropower, to dispatch within quick time during contingencies and sudden loss of renewable energy generation. Procedures to account for generation outages (N-1 contingencies) exist with the system operators since the advent of interconnections and are developed to adopt the relevant North American Electric Reliability Corporation (NERC) standards to maintain reliability of the grid. FERC has approved NERC's agreement with the eight regional reliability organizations to ensure and enforce the compliance of operations with the reliability standards [4]. These procedures are based on theory of interconnected networks, physics of power systems and their control, and practical experiences in grid operation. The generation variability introduced by interconnection of renewable variable output energy sources requires a different approach as compared to the one based on dispatchable generator units [5,6].

Hydroelectric generation can be very effectively utilized in an optimization framework to accommodate the increasing penetration of renewable energy resources [5,6,8–10]. The pattern of electricity generation using hydroelectric generation and other renewable sources in the U.S. is shown in Fig. 1. The inference that can be drawn is that hydropower technology is the largest producer of clean energy in the U.S. It is expected, that renewable generation will continue to increase for the foreseeable future. Coordinated hydro power generation can improve the grid reliability [11]. In general, the growth in installed hydropower generation has fluctuated in the past few decades but it is projected to increase in the near future as noted in the Hydropower Vision by the Department

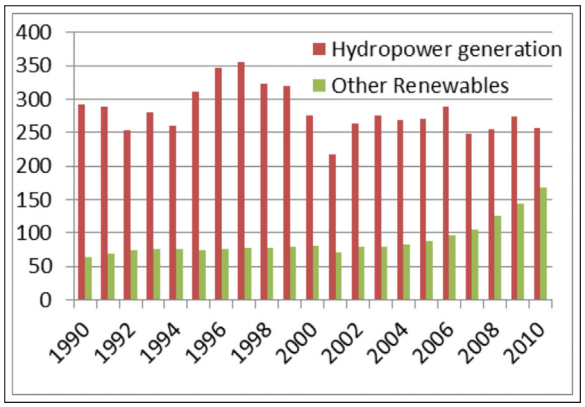

Fig. 1. Electricity generation by hydro and renewable energy sources in the U.S. (*X*-axis: year and *Y*-axis: electricity generated in million MWh).

of Energy (DOE) [12]. Fig. 2 shows the fraction of electricity generated by all hydropower technologies (including PSH) for leading hydropower producing countries of the world [7]. According to the National Hydropower Association (NHA) in the U.S. PSH plants exist at 40 locations with installed capacity of approximately 22,000 MW and future plants at 60 new locations with a total of 51,130 MW are pending approvals [13]. The magnitude of storage potential using PSH technologies is of significant value. Other potential attributes of AS-PSH are frequency regulation in both pumping and generating modes, grid scale inertial response based storage, part load pumping and ancillary services (load following, voltage support, and flexible spinning reserve). The utilities in Japan were the first to realize the benefits of adjustable speed pumped storage [14].

Specific benefits of AS-PSH operation include improvement of system stability, better dynamic performance, use of multi-level converters to enhance operational efficiency, enhanced market prices, and smoothing of renewable energy are demonstrated for the European and Asian grids in [15–20]. However, the aforementioned benefits are applicable to any grid interconnections and are generalizable. Besides generating dispatchable power, hydroelectric power plants were historically utilized to provide regulation services and they can act as sources of spinning reserves. PSH can also serve as a critical resource for black start procedures and system restoration hence is an added advantage. The fast ramp rates and quick response of hydroelectric power plants make them a viable source as providers of balancing services and daily load following [16]. The quantification of value of AS-PSH to the grid as a critical task was identified and presented in [21,22]. For the quantification of value, especially rotational inertia-like response that the AS-PSH can provide to the grid, accurate modeling is necessary for simulation, assessment, and market frameworks. After a rigorous assessment of existing models in hydroelectric power engineering a DOE report identified two major research gaps namely, research and modeling of AS-PSH and modeling of Ternary PSH units [23]. The challenges associated with PSH are high investment cost, licensing procedures, and availability of water especially with power generation being a lower priority.

Dynamic models for AS-PSH available for power system stability analysis are presented by treating the water column as a rigid (transient) and elastic (long term dynamics) body both described in [24,25]. The model proposed uses conventional hydro turbine and pump head-flow curve with gate control for generation and pump mode respectively. Models are also proposed based on combinations whether the plants have a common tunnel and multiple penstocks [26,27]. One of the fundamental publications in analyzing the transient response of AS-PSH based on a Hitachi design that is operational in Japan is presented in [28]. The operational and

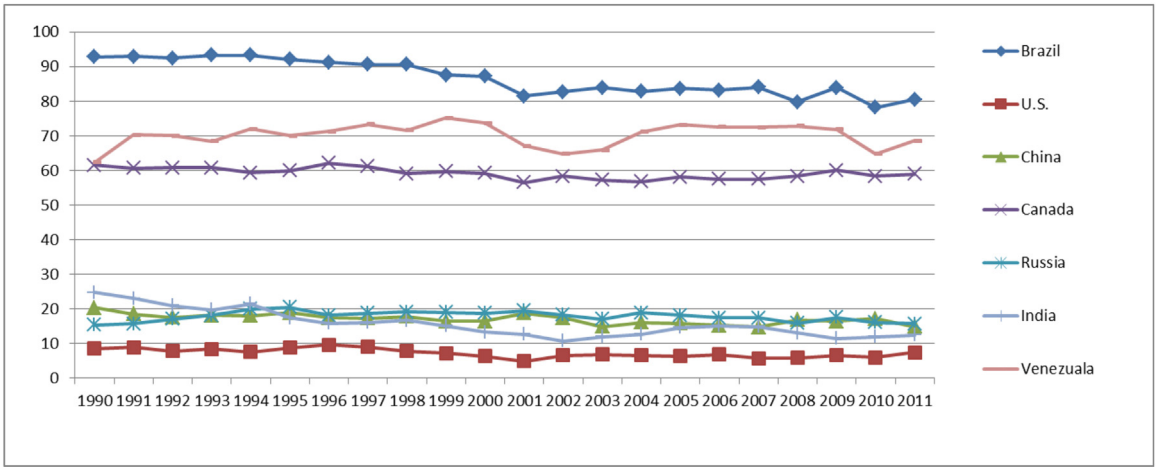

Fig. 2. Percentage of hydro power generation to the total electricity generation for leading hydro producers of the world (*X*-axis years and *Y*-axis total fraction of hydroelectric generation) [7].

control philosophy during both generation and pump mode in the Hitachi design is based on 'active power control'. Two noteworthy contributions of this paper (1) controls are similar for both modes in steady state whereas they vary considerably while in transient state and (2) advantage of active power based control over rotation speed based control. Reference [29] explains the design considerations and control implementation for both generation and pump modes of a pioneering AS-PSH project at Okawachi, Japan in 1993. The design considerations are based on active power control, speed optimization and stability, and frequency stability of the grid.

It is necessary that the active power and speed controls be compatible with one another for stable operation of the AS-PSH. The control strategies of AS-PSH and its implementation along with the advanced governor design are of paramount importance for successful operation. The advancement of the AS-PSH technology requires novel control implementations and suitable testing mechanisms. As described and implemented in [27,30], there are two primary techniques of AS-PSH control namely, active power and frequency controls. Numerous control algorithms have been proposed in this regard to optimize the performance of AS-PSH and tested using both real-time and non-real-time (or offline) simulation environments [7,23,24,26–32]. Real-time cosimulation of the hydrodynamic and power system events to assess transient stability is regarded as one of the most accurate means of understanding the interaction of the two energy systems [33–35]. There are several other advantages of performing real-time simulation of AS-PSH as proposed here namely, performing hardware-in-the-loop of power converters, machines, and controllers for testing under real world conditions.

Multiple modeling efforts of PSH plants to date are based on ordinary differential equations for the hydraulic circuit, reservoir, penstock, turbine, etc. [31,36–39]. However, AS-PSH modeling based on ordinary differential equations may not be adequate for studying transients in power systems. The main reason is the transfer function coefficients obtained from ordinary differential equations are not valid in the milli-second time periods. Hence, an AS-PSH model based on coupled partial differential equations is used for a co-simulation in a real-time environment [22]. Transient stability analysis of a test system is examined on the virtue of fast active power control AS-PSH. A thorough account of the development of the AS-PSH model and associated control models is also provided.

Section 2 describes the AS-PSH configuration modeled in this paper. Additionally, modeling attributes of the AS-PSH for both generation and pump modes of operation based on a novel technique are briefly described in this section. Section 3 describes the IEEE 14 bus test system modeled in the Digital Real-Time Simulator (DRTS) along with a description of the simulation. Section 4 describes several scenarios that were simulated with pertinent observations to assess the stability of the test system under fault conditions. Section 5 summarizes the results of the analysis performed in this study.

2. Adjustable speed pumped storage hydro model

The objectives and applications of developing the real-time AS-PSH model in this paper are multifold and are based on extensive literature review as presented in Section 1. In this paper the first two objectives are demonstrated and the rest are noted as information.

(i) Creating physics-based, vendor-neutral generic model that can provide a dynamic and transient response in real-time.
(ii) Capability of simulating both turbine and pump modes of operation of AS-PSH.
(iii) Capability to co-simulate the hydro-dynamics with other domains i.e., electrical, mechanical, and thermal (power converters) at microsecond level time-steps.
(iv) Demonstrate the provision of both real-time energy and ancillary services.
(v) Capability of providing an environment for Controller-Hardware-In-the-Loop (CHIL), Hardware-In-the-Loop (HIL), and Power-Hardware-In-the-Loop (PHIL) to serve as a verification and validation platform.

AS-PSH units differ from conventional hydroelectric power plant single-speed salient pole synchronous generating units in two major ways – (1) recirculation of water between the upper and lower reservoir and (2) the reversible doubly-fed induction electric motor/generator connected to a pump/turbine water wheel, and the rotor excitation with power electronic converters. Most practical AS-PSH configurations use the Francis water wheels with wicket gates with suitable control configuration. This design philosophy is similar to the Type 3 wind turbines based on power electronic converters that assist in controlling the operation of the Doubly Fed Induction Machine (DFIM) [40]. It is important to note, that in DFIM topologies the rotational speed of the generator is fully decoupled from the grid frequency unlike conventional PSH (synchronous generator based) plants. The architecture of the AS-PSH allows three modes of operation with – generation, pumping, and idling capabilities [41]. In fact, with AS-PSH it is possible to provide both load following and frequency regulation. All these modes

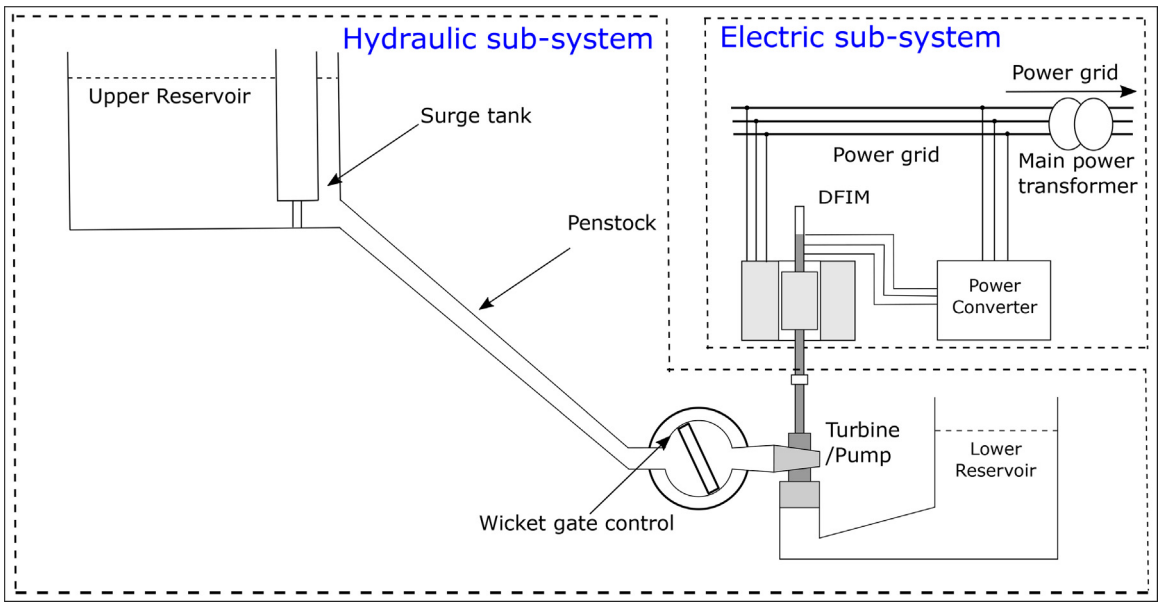

Fig. 3. A pictorial representation of the AS-PSH power plant.

of operation can be optimally utilized to enhance market participation and hence increase revenue. Fig. 3 depicts the AS-PSH modeled and presented in this study.

AS-PSH models have two main subsystems – hydraulic and electric. The hydraulic subsystem includes upper and lower reservoirs, surge tank (typically used in modern designs), penstock, wicket gates, unit shut-off valves, governor, and turbine/pump. The electric subsystem consists of the reversible electric motor/generator, power converters (machine side and line side), auxiliary power supply systems, and main power transformer. The rating of the power converter is a function of the desired range of speed adjustment of AS-PSH unit. A sample derivation of the power converter rating is provided in [42].

The objective of modeling AS-PSH hydraulic circuit was to obtain a physics based representation of the mechanical, rotational inertia, and hydrodynamic loads during both turbine and pump mode of operation. The methodology for modeling adopted in the proposed case is based on coupled partial differential equations solved for the expected boundary conditions between the different components of the hydraulic subsystem. The basis of the modeling is the water flow dynamic equations in a water conduit given the time evolution of the pressure head $H(x,t)$ and fluid velocity $U(x,t)$. These equations are also alternatively known as 'water hammer equations' [42] and are summarized in (1) and (2) –

$$\frac{\partial H}{\partial t} = -U\frac{\partial H}{\partial x} - \frac{a^2}{g}\frac{\partial U}{\partial x} \tag{1}$$

$$\frac{\partial U}{\partial t} = -U\frac{\partial U}{\partial x} - \frac{fU|U|}{2D} - g\frac{\partial H}{\partial x} \tag{2}$$

In (1) and (2), $H(x,t)$ is pressure head, $U(x,t)$ is the fluid velocity, a is the pressure wave velocity, g is gravitational acceleration, D is internal diameter of the pipe, and f is a friction factor. In addition to (1) and (2), two more equations are critical for the formation of the AS-PSH models and these are related to the flow velocity at the turbine wicket gate and the turbine mechanical power. The flow velocity of a particle under acceleration due to gravity at any point can be determined from basic laws of motion and is given in (3). Referring to Fig. 4 and considering the fact that the water flow in the turbine is controlled by the gates located at the base of the penstock, applying the water hammer equations all the locations numerically designated for the hydraulic conduit. Stable solutions are obtained

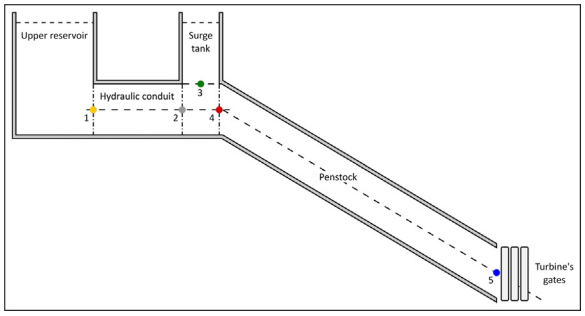

Fig. 4. Hydraulic circuit of the AS-PSH with locations to solve boundary conditions highlighted.

based on suitable boundary conditions is the proposed approach. Combining all the five solutions representing the five hydraulic segments provides the transfer function between the upper reservoir and the turbine gates i.e., between locations 1 and 5 as shown in Fig. 4.

$$v = \sqrt{2gh} \tag{3}$$

$$U_5 = \bar{G}\sqrt{\bar{H}_5} \tag{4}$$

where the function $\bar{G}$ defines the control operation of the opening and closing of the wicket gates. Wicket gates are typically provided by the turbine manufacturer.

Using the law of conservation of energy, the mechanical power of the turbine is equal to the power transferred from the fluid. The power transferred from the fluid computed as fluid velocity times pressure at the turbine gate less the no-load losses that are accounted using a damping term that is proportional to speed changes. With these considerations the mechanical power can be written as:

$$\bar{P_m} = A_t\left(\bar{U_5} - \bar{U_{NL}}\right)\bar{H_5} - D_{turb}\left(\bar{\omega} - \bar{\omega_o}\right) \tag{5}$$

where the constants A_t and D_{turb} are turbine specific values provided by the manufacturer. The five equations (1)–(5) describe the dynamics associated with the hydraulic subsystem of the AS-PSH including the water hammering effects.

There are several techniques for solving a set of partial differential equations. Under conditions where simplifying assumptions can be made, the integral transform method allows an analytical treatment of the problem. In particular, the Laplace transform with respect to time is a suitable candidate. When simplifications cannot be made, the full equations can be solved using a technique that transforms the 'water hammer' equations (1) and (2) to a set of ordinary differential equations (ODE) that are then solved using established numerical methods for solving ODEs, this method is known as 'the method of characteristics'. A third method consists of solving the partial differential equations directly, using the finite difference method. There are other solution approaches, but these three methods are the most commonly used. The choice of the model and solution method usually depend on the required fidelity of the model in describing the important physics effects, the numerical stability and numerical errors introduced by the method, and computation overhead (based on simulator type and its capacity). The solution method used in this paper to solve the partial differential equations is the integral transform method. Noting that the pressure wave velocity a in Eq. (1), typically 1000 m/s, is much higher than the fluid velocity U, usually 10 m/s, the terms $U\frac{\partial H}{\partial x}$ and $U\frac{\partial U}{\partial x}$ in Eqs. (1) and (2) can be neglected. A further simplification can be obtained by neglecting the friction term in Eq. (2). Approximations of the effect of the friction loss term can be added to the frictionless solution afterwards [43]. The frictionless 'water hammer' equations can be expressed as:

$$\frac{\partial H}{\partial t} = -\frac{a^2}{g}\frac{\partial U}{\partial x} \tag{6}$$

$$\frac{\partial U}{\partial t} = -g\frac{\partial H}{\partial x} \tag{7}$$

Using the integral transform method and applying Laplace transform to H and U:

$$H_L(x,s) = \int_0^\infty e^{-st}H(x,t)dt \tag{8}$$

$$U_L(x,s) = \int_0^\infty e^{-st}U(x,t)dt \tag{9}$$

Assuming the initial conditions of $H(x,0) = U(x,0) = 0$; and combining the above equations:

$$\frac{\partial H}{\partial t} = sH_L(x,s) = -\frac{a^2}{g}\frac{\partial U_L(x,s)}{\partial x} \tag{10}$$

$$\frac{\partial U}{\partial t} = sU_L(x,s) = -g\frac{\partial H_L(x,s)}{\partial x} \tag{11}$$

Substituting $\alpha = \frac{g}{a^2}$, the transformed water hammer equations have a general form as:

$$H_l(x,s) = -\frac{C_1}{\sqrt{g\alpha}}\sinh\left(\frac{sx}{a}\right) - \frac{C_2}{\sqrt{g\alpha}}\cosh\left(\frac{sx}{a}\right) \tag{12}$$

$$U_l(x,s) = C_1\cosh\left(\frac{sx}{a}\right) + C_2\sinh\left(\frac{sx}{a}\right) \tag{13}$$

where C_1 and C_2 are the constants determined by the boundary conditions. These equations represent the simplified form of water hammer equations and can be applied to different locations i.e., (1)–(5) in Fig. 4.

Applying the simplified water hammer equations to the top and bottom of the penstock:

$$U_{L4} = U_L(0,s) = C_4 \tag{14}$$

$$H_{L4} = H_L(0,s) = -\frac{C_5}{\sqrt{g\alpha}} \tag{15}$$

At the downstream end of the penstock, marked as location 5 in Fig. 4:

$$U_{L5} = U_L(L,s) = C_4\sinh\left(\frac{sL}{a}\right) + C_5\sinh\left(\frac{sL}{a}\right) \tag{16}$$

$$H_{L5} = H_L(L,s) = -\frac{C_5}{\sqrt{g\alpha}}\cosh\left(\frac{sL}{a}\right) - \frac{C_5}{\sqrt{g\alpha}}\sinh\left(\frac{sL}{a}\right) \tag{17}$$

Replacing C_4 and C_5 using the equations above and rearranging the terms based on trigonometric identities:

$$H_{L5} = H_{L4}\cosh(sTe) - \frac{U_{L1}}{\sqrt{g\alpha}}\sinh(sTe) \tag{18}$$

$$U_{L5} = U_{L4}\sinh(sTe) + \sqrt{g\alpha}H_{L4}\sinh(sTe) \tag{19}$$

where $T_e = \frac{L}{a}$ is the penstock elastic time. Now the friction loss is accounted as a first order approximation and then subtracting it from the pressure head as computed above:

$$\frac{f|U_{L5}|U_{L5}}{2D} \approx \frac{f|U_{L50}|U_{L5}}{2D} = k_{L5}U_{L5} \tag{20}$$

where U_{L50} is the steady state value of flow velocity at the penstock downstream end, and $k_{L5} = \frac{f|U_{L50}|U_{L5}}{2D}$ is the friction factor. Inserting the friction terms for from the head:

$$H_{L5} = H_{L4}\cosh(sTe) - \frac{U_{L1}}{\sqrt{g\alpha}}\sinh(sTe) - k_{L5}U_{L2} \tag{21}$$

$$U_{L5} = U_{L4}\sinh(sTe) + \sqrt{g\alpha}H_{L4}\sinh(sTe) \tag{22}$$

Eqs. (21) and (22) provide the flow velocity and pressure head at the penstock downstream location i.e., at the turbines gates, as a function of their values at the penstock upstream location, i.e., where the water conduit and the surge tank meet. This procedure allows the set-up of the boundary conditions when several devices are connected in a hydraulic network such as in the model shown in Fig. 4. Converting these equations to the per unit format for ease and dropping the term 'L' for ease. Additionally, normalizing the penstock impedance and friction factor and expressing in terms of deviation terms we get:

$$\bar{h_5} = \bar{h_4}sech(sTe) - Z_p\bar{u_5}\tanh(sTe) - k_{fp}\bar{u_5} \tag{23}$$

$$\bar{u_4} = \bar{u_5}\cosh(sTe) + \frac{1}{Z_p}\bar{h_5}\tanh(sTe) \tag{24}$$

where $\bar{h_5} = \bar{H} = \bar{H_0}$ and $\bar{u_4} = \bar{U} - \bar{U_0}$.

In a similar manner, solving the simplified at all locations 1 through 5 as shown in 4 and solving the boundary level conditions with the suitable values of head and flow the final transfer function can be obtained at location 5 and is shown below:

$$T(s) = \frac{\bar{u_5}}{\bar{h_5}} = \frac{-\left(1 + \frac{\left[Z_c\tanh(sTe_c) + k_{fC}\right]}{1 + \left[Z_c\tanh(sTe_c) + k_{fC}\right]sT_{ST}}\frac{\tanh(sTe_P)}{Z_P}\right)}{\frac{\left[Z_c\tanh(sTe_c) + k_{fC}\right]}{1 + \left[Z_c\tanh(sTe_c) + k_{fC}\right]sT_{ST}} + Z_P\tanh(sTe_P) + k_{fP}} \tag{25}$$

$$\tanh(x) = x - \frac{x^3}{3} + \frac{2x^5}{15} + \frac{17x^7}{315} + \cdots \tag{26}$$

$$\begin{aligned}\tanh(sTe_C) &\approx sTe_C\\ \tanh(sTe_P) &\approx sTe_P\end{aligned} \tag{27}$$

$$T(s) = \frac{\bar{u_5}}{\bar{h_5}} = \frac{-\left(1 + \frac{\left[Z_c sTe_c + k_{fC}\right]}{1 + \left[Z_c sTe_c + k_{fC}\right] sT_{ST}} \frac{sTe_P}{Z_P}\right)}{\frac{\left[Z_c sTe_c + k_{fC}\right]}{1 + \left[Z_c sTe_c + k_{fC}\right] sT_{ST}} + Z_P sTe_P + k_{fP}} \quad (28)$$

$$T(s) = \frac{\bar{u_5}}{\bar{h_5}} = \frac{-(Z_P + Z_P \left[Z_C sTe_C + k_{fC}\right] sT_{ST} + \left[Z_C sTe_C + k_{fC}\right] sTe_P)}{Z_P \left[Z_C sTe_C + k_{fC}\right] + \left(Z_P sTe_P + k_{fP}\right)\left(1 + \left[Z_C sTe_C + k_{fC}\right] sT_{ST}\right) Z_P} \quad (29)$$

The transfer function of interest for the entire hydraulic segment as shown in Fig. 4 at the position 5 is derived as:

$$T(s) = -\frac{n_0 + n_1 s + n_2 s^2}{d_0 + d_1 s + d_2 s^2 + d_3 s^3} \quad (30)$$

The coefficients of the transfer function are: $n_0 = Z_p$, $n_1 = Z_p k_f c T_{ST} + k_f c T_{ep}$, $n_2 = Z_p k_{fC} T_{ST} T_{ec} + Z_c T_{ec} T_{ep}$, $d_0 = Z_p(k_{fP} + k_{fC})$, $d_1 = Z_{pk} k_{fP} k_{fC} T_{ST} + Z_p Z_C T_{eC} + Z_p^2 T_{ep}$, $d_2 = Z_p^2 k_{fC} T_{eP} T_{ST} + Z_p Z_C T_{ec} T_{ST} T_{eC} k_{fP}$, and $d_3 = Z_p^2 Z_C * T_{ST} T_{eC} T_{eP}$. Variables T and Z are the time constant and impedance of channels denoted by the subscripts. Subscripts 'P' and 'C' identify penstock and conduit variables. The set of equations (4), (5), and (30) now represents the hydrodynamic model that can be used in simulation models of AS-PSH systems.

3. Models of DFIM and governor controls

An advantage of a DFIM in the PSH configuration, such as the one under consideration, is that it requires a line side converter with MVA ratings significantly less than the MW rating of the DFIM. Because cost is a major driver especially for AS-PSH units with ratings greater than 100 MW, the use of the machine-side converter has reduced initial cost as compared to a converter fed machine with 100% line-side power conversion. With a DFIM AS-PSH unit the machine-side converter rating is a function of the +/− range of speed operation sought for adjustable speed operation. A rule of thumb in determining the rating of the converter for DFIM – for a range of +30% to −30% of slip variation, a power converter of rating equal to 30% of the machine is needed [42]. Total speed variations in the operation of AS-PSH in the range of +4% and −13.8% are reported in practice [21]. The total power delivered to the grid from an AS-PSH unit is equal to the summation of the power drawn from the stator and rotor, both. Independent control of active and reactive power of DFIM is possible by the means of its power converter. Using the space vector representation a physics-based model of a DFIM is given by the following equations, with reference to Fig. 5. The $d-q$ frame of reference is chosen here as it is one of the most common implementations. Conventional naming of voltages, currents, inductances, and resistances are used with subscript s for stator variables and subscript r for rotor variables. This is a standard convention used in electric power system literature to address stator and rotor side variables for creating theoretical framework. In the $d-q$ frame of reference the rotor currents can be expressed as:

$$i_{rd} = \frac{3}{2} i_{ra} \cos(\omega_o t - \psi) - \frac{3}{2}(i_{rb} - i_{rc}) \sin(\omega_o t - \psi) \quad (31)$$

$$i_{rq} = \frac{3}{2} i_{ra} \sin(\omega_o t - \psi) - \frac{3}{2}(i_{rb} - i_{rc}) \cos(\omega_o t - \psi) \quad (32)$$

Finally, the rotor shaft can be modeled as a single mass or a two-mass shaft to represent coupled turbine and generator shafts. For a single mass shaft the dynamic equation when operating in turbine mode is:

$$\frac{d\bar{\omega_m}}{dt} = \frac{1}{2H_s}(\bar{T_m} - \bar{T_e}) - D_f \bar{\omega_m} \quad (33)$$

where $\frac{d\theta}{dt} = \bar{\omega_m}$ is the angular velocity of the machine. H_s is the combined inertia of the generator/motor and turbine/pump. $\bar{T_m}$ and $\bar{T_e}$ are the mechanical and electrical torque of the machine in per unit, respectively. The total power delivered to the grid can be computed as:

$$P_{total} = (P_{ms} - P_{mr}) = (1 - slip) * P_{ms} \quad (34)$$

The DFIM equations above are written in a format amenable to both field-oriented and active power control. The governor controls used in this study are based on active power controls. The stator and rotor side converter controls utilize the real and reactive components of currents to provide desired power output from both stator and rotor, respectively [42]. The implementations of hydro-governor control for turbine mode, pump mode, hydrodynamics, and DFIM and its controls in RTDS® (a commercially available real-time simulator) are shown in Figs. 6–9 respectively. The integrators used in the hydro-governor controls for turbine, pump, and hydrodynamics of operation as shown in Figs. 6–8 have a time constant of 0.01 s. The hydrodynamic constants shown in Fig. 8 are – $a0 = 3.267$, $a1 = 0.02668$, $a2 = 0.002668$, $b1 = 0.0042$, and $b2 = 0.004075$). The look up table used in the hydrodynamics as shown in Fig. 8 is elaborated in Table 1. The units for X and Y are in p.u.:

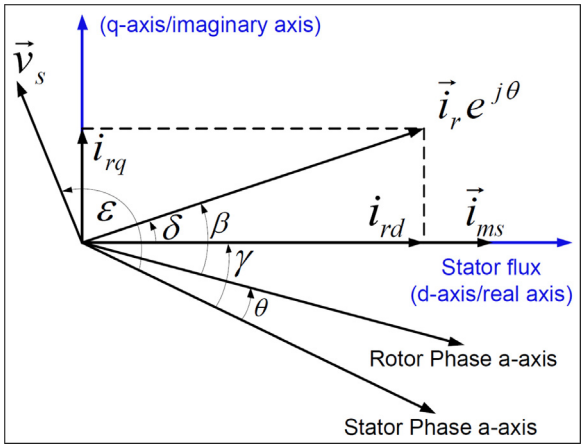

Fig. 5. Space vector graphical representation with rotor current 'oriented' in the direction of stator flux.

4. Real-time co-simulation

4.1. Real-time co-simulation test set up

Fig. 9 shows the connectivity of the IEEE 14 bus test system. The data required for modeling this system is available [44]. Fig. 10 represents the actual power systems representation of the IEEE 14 bus test system with the AS-PSH model. This test system is well-established for testing research results and is based on a legacy American Electric Power system. Bus no. 2 in this system has a 40 MW generation capacity of which a 25 MW AS-PSH plant is substituted for this co-simulation. The rating of AS-PSH can be changed as required. The AS-PSH connected to the IEEE 14 bus test system is modeled in a digital real-time simulator and is based on the mathematical formulation described in Sections 2 and 3. The transient response of the AS-PSH is obtained via co-simulation with standard electrical events based on electrical faults. The real-time model of AS-PSH consists of standard modules i.e., hydro-governor,

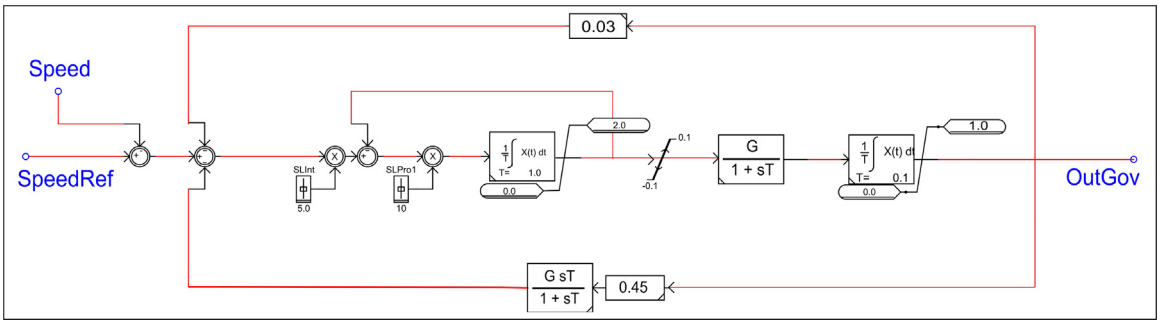

Fig. 6. Hydro-governor controls for turbine mode of operation.

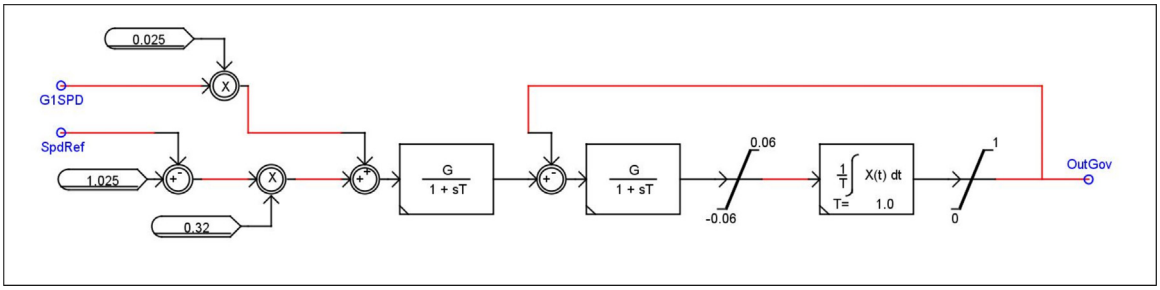

Fig. 7. Hydro-governor controls for pump mode of operation.

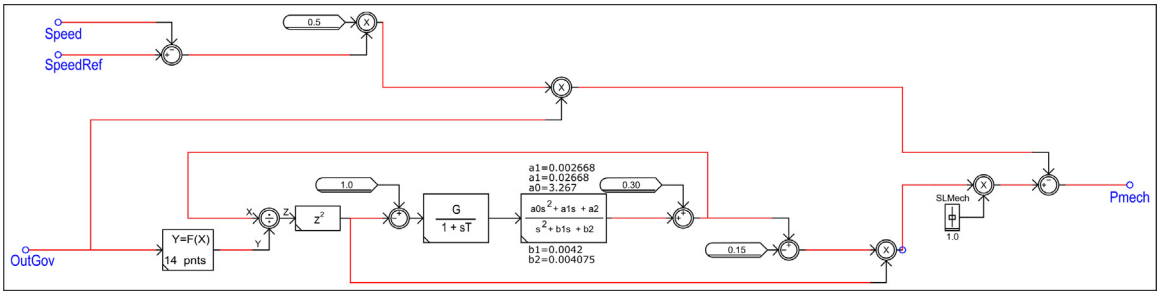

Fig. 8. Hydrodynamic simulation developed based on the theory discussed in Section 2.

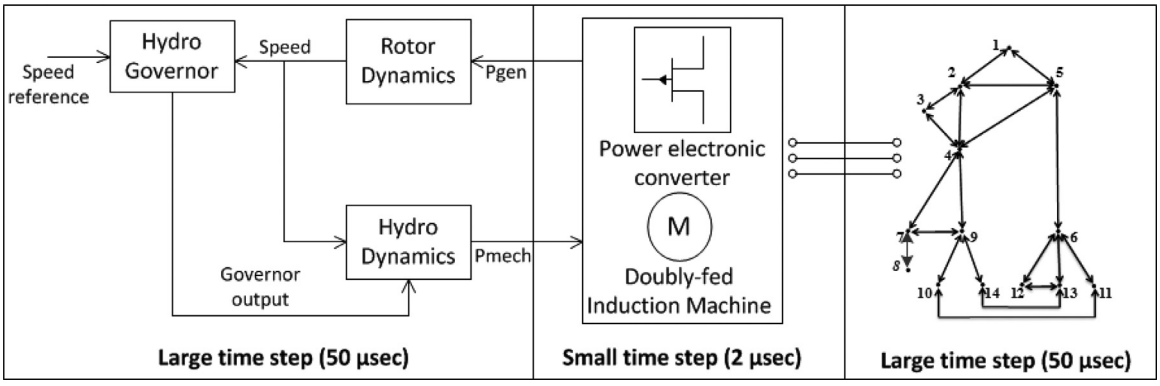

Fig. 9. Real-time co-simulation of AS-PSH and IEEE 14 bus test system.

hydrodynamics, doubly-fed induction machine, and power electronic converter as shown. Fig. 9 shows a block diagram of the physics based AS-PSH model developed and implemented in real-time environment for this study. Faults are applied at bus no. 2 to capture the response of the AS-PSH to these events.

The real-time simulation consists of the hydro-governor, hydrodynamics, and the IEEE 14 bus test system simulated in the 'large time-step' whereas the power electronic converter and the DFIM are simulated in the 'small time-step'. Both 'large and small time-step' modules are solved in the RTDS® with the resolution of 50 and 2 µs, respectively. A unique aspect of the proposed work; i.e., multi-scale real-time models of 'large' and 'small' time steps, and the mathematical formulation adopted to generate them, are necessary to generate accurate responses. Fault scenarios (both balanced and unbalanced) are simulated and presented in this section. The faults presented in this paper are of three cycle duration. Faults

Table 1
Look up table for the hydrodynamic simulation shown in Fig. 8.

Sr.No.	X	Y
1	−0.1	0.005
2	0	0.01
3	0.1	0.05
4	0.2	0.15
5	0.3	0.27
6	0.4	0.38
7	0.5	0.49
8	0.6	0.595
9	0.7	0.696
10	0.8	0.797
11	0.9	0.898
12	1	0.999
13	1.1	1.09
14	1.2	1.19

are typically cleared within a specific time (so-called self-clearing faults) determined by the protective relay settings, fault identification, and circuit breaker operation. Three cycle fault clearing time provides an understanding of the momentary disturbances and its impacts in the power systems. The results of these simulations indicate transient stability of the IEEE 14 bus test system under two configurations. The first configuration is the IEEE 14 bus test system with a conventional generator connected at the bus no. 2. For the second configuration, the conventional generation is replaced by an AS-PSH unit. The transient responses of these two configurations are recorded and presented in the next subsection. It should be noted that Fig. 9 summarizes the details for the AS-PSH unit with DFIM only, whereas a similar picture for the conventional generator is possible with minute details. The figure providing details of the conventional generator are not shown for the sake of conciseness. The location of faults will determine the magnitude and nature of transients that the AS-PSH will experience and hence respond to.

4.2. Real-time co-simulation results

A real-time co-simulation of the hydrodynamics (representing the hydraulic circuit) and power systems is performed. The first configuration with conventional hydropower generation, based on synchronous generator, is operated at a fixed speed i.e., the synchronous speed. For the second configuration, with the AS-PSH, the co-simulation is started with the DFIM operating in the 'lock' model. This implies, that the DFIM is started at a fixed speed of 1.05 p.u. After 10 s of fixed speed operation; the DFIM is switched to the 'free' mode in which the swing equation determines the speed of operation. This ensures the simulation stability of the grid leading to accurate results. For the sake of simplicity, the response of AS-PSH for the generation mode of operation is presented. However, the model developed here is capable of operation in both generation and turbine modes as described in Section 2.

Single-line to ground (SLG), two-line to ground (LLG), and three-line to ground (3LG) faults are applied at bus no. 2. In the co-simulations, the following variables are recorded: (1) electrical (real power, reactive power, and frequency) and (2) hydro (speed, mechanical torque, electrical torque, governor output, etc.) and results are shown in Figs. 11–14. The output of the hydrodynamic circuit is 'Pmech' represents the boundary variable of the co-simulation between the hydro and electric circuits. The response of the conventional generator and AS-PSH unit in all figures is shown in blue and green, respectively. For the three-fault scenarios, the transient and dynamic response and system stability is demonstrated by the exponentially damped oscillations of real power. The scenarios with a conventional generator show lower frequency swings immediately following the application of a fault. Both generator types demonstrated a dampening of power and frequency swings. The largest frequency swing (61 Hz) is observed for the LLG fault for the AS-PSH operation. In general, the two configurations are critically damped and hence the responses become stable within a few seconds. The power and frequency oscillations with AS-PSH, settle down to steady state in a relatively short time as compared to the case with the conventional generator.

The reactive power responses are significantly dependent on the ratings and controls of the power converters used and hence the difference in responses. The controls of power converters can be suitably tuned to obtain optimal voltage support. DFIM configurations use power converters with ratings that are a fraction of the machine rating itself as described in [45].The reactive power response of the AS-PSH is similar in all fault scenarios. Fig. 14 shows the speed of AS-PSH, mechanical, and electrical torque while responding to a 3LG fault. The mechanical torque shown is the

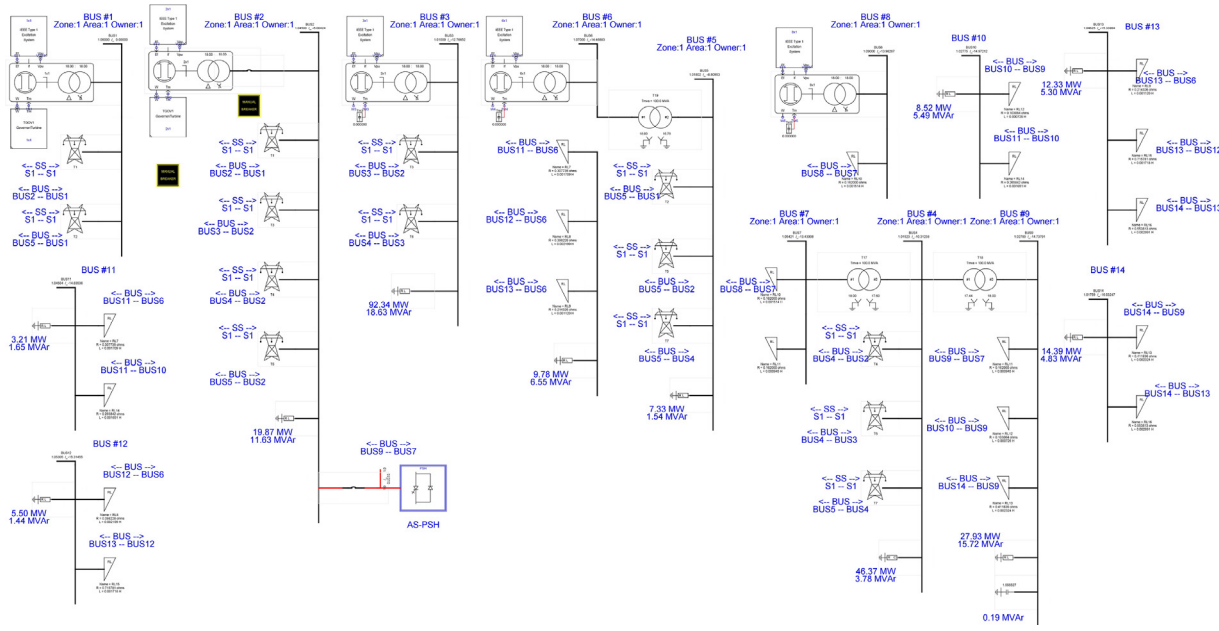

Fig. 10. Real-time model of the IEEE 14 bus test system.

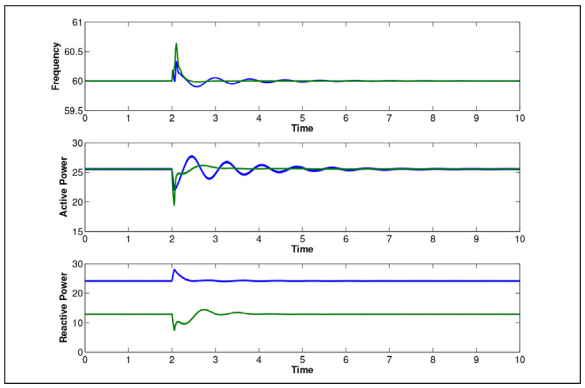

Fig. 11. Transient response of AS-PSH and a conventional generator to LG fault.

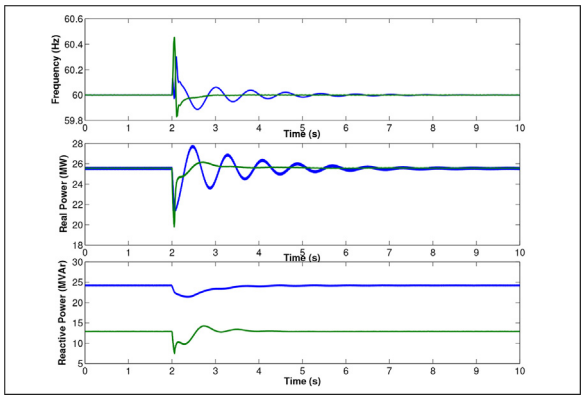

Fig. 12. Transient response of AS-PSH and a conventional generator to LLG fault.

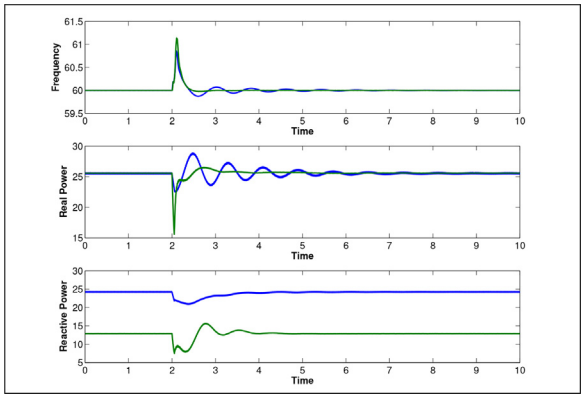

Fig. 13. Transient response of AS-PSH and a conventional generator to 3LG fault.

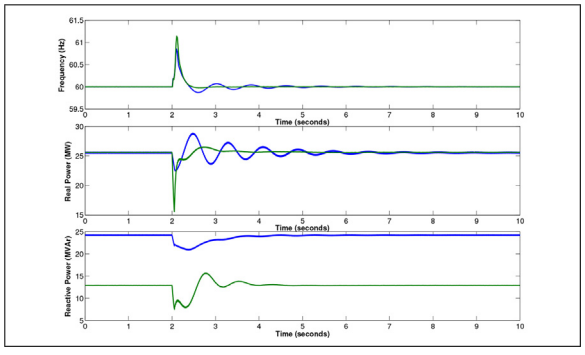

Fig. 14. Rotor speed, mechanical torque, and electrical torque of the AS-PSH with response to a 3LG fault in the test system.

response in the hydraulic circuit to the 3LG fault. Based on the magnitude of the dip in the real power output of the AS-PSH, the hydro-governor controls the gate operation and increases the flow resulting in the speed deviation shown. The electrical torque oscillation shown, is similar to a typical DFIM response. The co-simulation of hydraulic and power systems allows the model to capture the actions of governor, water flow and velocity, and other intricate details. Additionally, with the same fault conditions the AS-PSH operating in the pump mode with a speed of 0.95 p.u. is connected and the transient responses are captured and shown in Fig. 15. Real power transients of the AS-PSH operating in the pumping mode for all three faults (LG, LLG, and 3LG) are captured. Fig. 16 shows the short circuit current contributions of AS-PSH and conventional synchronous generator in response to a 3LG fault. Also, Fig. 17 shows the rotor angle oscillation for both AS-PSH and conventional synchronous generator and both curves demonstrate transient response to a 1LG fault. Fig. 18 shows the details of voltage

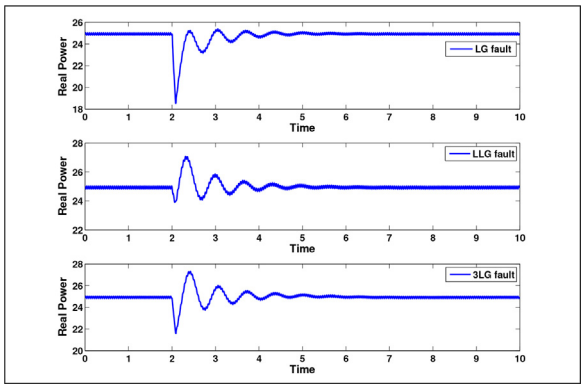

Fig. 15. Real power transients of the AS-PSH operating in the pumping mode for all three faults (LG, LLG, and 3LG).

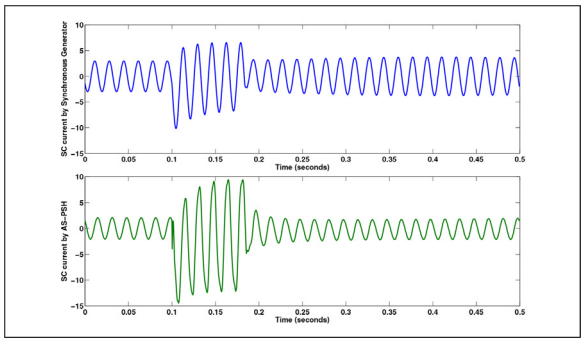

Fig. 16. Short circuit current (in kA) contributions of AS-PSH and conventional synchronous generators during the 3LG fault.

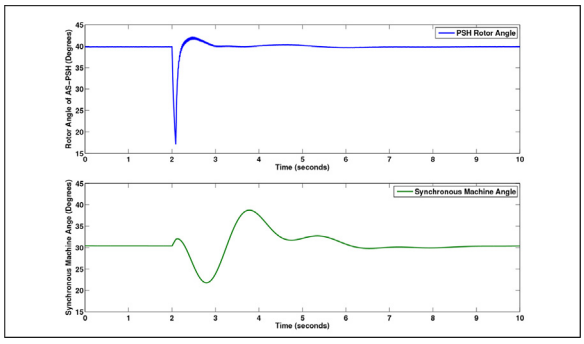

Fig. 17. Rotor angle plots of AS-PSH and conventional generator.

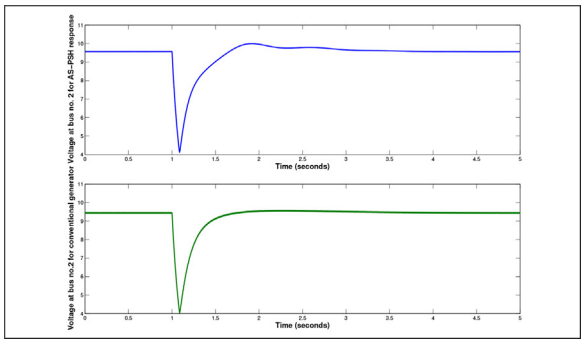

Fig. 18. Voltage measured in kV at bus no. 2 for AS-PSH and conventional generator for 3LG fault.

measured at bus no. 2 before and after a 3LG fault for both AS-PSH and conventional generator. The voltage stability demonstrated by the conventional generator is superior to that of the AS-PSH due to low ripples. Details of every variable from the hydraulic circuit are not shown for the sake of conciseness. These results can also be used to evaluate the impacts on plant structural loading during such transient events.

5. Concluding remarks

This paper describes a modeling effort of a DFIM AS-PSH unit using partial differential equations together with water-hammering equations of flow and head. The water-hammer equations are solved using the integral transform method. This technique provides a unique advantage of solving partial differential equations, such as the ones here, with numerically stability and accurate results. The AS-PSH model is capable of demonstrating several modes of operation as observed in practice. A real-time co-simulation of hydro and power systems is performed and compares transient response of AS-PSH and conventional hydro generators. Transient stability is observed in the test system with AS-PSH for standard faults. Being a major grid level storage technology, the stability attribute is extremely essential, especially with growing renewable energy penetrations and reductions in total system inertia. The model also allows a unique environment to test controllers as well as power converter hardware in real-time. This testbed will hence act as a rapid prototyping environment for controllers and power converters. Future work involves the quantification of stability benefits of hydropower based storage systems, dynamic stability, and market analysis.

Acknowledgement

This work was supported by the U.S. Department of Energy, Hydropower Program under the project – PSH Transient Simulation Modeling at the Idaho National Laboratory, Idaho Falls, ID, USA.

References

[1] FERC: Landmark Orders – Order No. 888. http://www.ferc.gov/legal/maj-ord-reg/land-docs/order888.asp.
[2] M. Mohanpurkar, R. Ramakumar, Probability density functions for power output of wind electric conversion systems, in: 2010 IEEE Power and Energy Society General Meeting, 2010, pp. 1–7, http://dx.doi.org/10.1109/PES.2010.5590119.
[3] NERC, Essential reliability services task force measures frame-work report. http://www.nerc.com/comm/Other/essntlrlbltysrvcstskfrcDL/ERSTF%20Framework%20Report%20-%20Final.pdf.
[4] Organization and Procedures Manual for NERC Standing Committees, Tech. rep. http://www.nerc.com/comm/OC/Operating%20Manual%20DL/opman_20140825.pdf.
[5] J. Garcia-Gonzalez, D. la Muela, R.M. Ruiz, L.M. Santos, A.M. González, Stochastic joint optimization of wind generation and pumped-storage units in an electricity market, IEEE Trans. Power Syst. 23 (2) (2008) 460–468 http://ieeexplore.ieee.org/xpls/abs_all.jsp?arnumber=4494596.
[6] B. Vieira, A. Viana, M. Matos, J.P. Pedroso, A multiple criteria utility-based approach for unit commitment with wind power and pumped storage hydro, Electr. Power Syst. Res. 131 (2016) 244–254, http://dx.doi.org/10.1016/j.epsr.2015.10.024 https://www.sciencedirect.com/science/article/pii/S037877961500320X.
[7] Electricity production from hydroelectric sources (kWh) | Data | Table. http://data.worldbank.org/indicator/EG.ELC.HYRO.KH.
[8] G.W. Chang, M. Aganagic, J.G. Waight, J. Medina, T. Burton, S. Reeves, M. Christoforidis, Experiences with mixed integer linear programming based approaches on short-term hydro scheduling, IEEE Trans. Power Syst. 16 (4) (2001) 743–749 http://ieeexplore.ieee.org/xpls/abs_all.jsp?arnumber=962421.
[9] S.V. Papaefthymiou, E.G. Karamanou, S. Papathanassiou, M.P. Papadopoulos, A wind-hydro-pumped storage station leading to high RES penetration in the autonomous island system of Ikaria, IEEE Trans. Sustain. Energy 1 (3) (2010) 163–172 http://ieeexplore.ieee.org/xpls/abs_all.jsp?arnumber=5512672.
[10] M.T. Vespucci, F. Maggioni, M.I. Bertocchi, M. Innorta, A stochastic model for the daily coordination of pumped storage hydro plants and wind power plants, Ann. Oper. Res. 193 (1) (2012) 91–105, http://link.springer.com/article/10.1007/s10479-010-0756-4.
[11] R. Karki, P. Hu, R. Billinton, Reliability evaluation considering wind and hydro power coordination, IEEE Trans. Power Syst. 25 (2) (2010) 685–693 http://ieeexplore.ieee.org/xpls/abs_all.jsp?arnumber=5325712.
[12] Hydropower Vision: A New Chapter for America's 1st Renewable Electricity Source. http://energy.gov/eere/water/articles/hydropower-vision-new-chapter-america-s-1st-renewable-electricity-source.
[13] Anonymous, Challenges and Opportunities For New Pumped Storage Development, Tech. rep. http://www.hydro.org/wp-content/uploads/2014/01/NHA_PumpedStorage_071212b12.pdf.
[14] P. Donalek, H. Clarke, R. Nakata, J. Stein, Application of adjustable speed, doubly fed machines in pumped-storage and conventional hydro electric plants, in: Proceedings of the American Power Conference, 1993, April.
[15] J.-J. Simond, A. Sapin, D. Schafer, Expected benefits of adjustable speed pumped storage in the European network. Tech. rep., 1999 http://infoscience.epfl.ch/record/134070.
[16] J.P. Deane, B. Gallachóir, E.J. McKeogh, Techno-economic review of existing and new pumped hydro energy storage plant, Renew. Sustain. Energy Rev. 14 (4) (2010) 1293–1302 http://www.sciencedirect.com/science/article/pii/S1364032109002779.
[17] J.A. Suul, K. Uhlen, T. Undeland, et al., Variable speed pumped storage hydropower for integration of wind energy in isolated grids: case description and control strategies, in: Nordic Workshop on Power and Industrial Electronics (NORPIE/2008), June 9–11, 2008, Espoo, Finland, Helsinki University of Technology, 2008 https://aaltodoc.aalto.fi/handle/123456789/800.
[18] Y.-Y. Hsu, I.-W. Tao, Effect of a pumped storage plant on the generation reliability of the Taiwan power system, Electr. Power Syst. Res. 10 (3) (1986) 223–226, http://dx.doi.org/10.1016/0378-7796(86)90015-5 http://www.sciencedirect.com/science/article/pii/0378779686900155.
[19] Y. Huang, Q.P. Zheng, J. Wang, Two-stage stochastic unit commitment model including non-generation resources with conditional value-at-risk constraints, Electr. Power Syst. Res. 116 (2014) 427–438.
[20] L.J. Duque, E.D. Castronuovo, I. Sánchez, J. Usaola, Optimal operation of a pumped-storage hydro plant that compensates the imbalances of a wind power producer, Electr. Power Syst. Res. 81 (9) (2011) 1767–1777, http://dx.doi.org/10.1016/j.epsr.2011.04.008 https://www.sciencedirect.com/science/article/pii/S0378779611000940.
[21] V. Koritarov, L. Guzowski, J. Feltes, Y. Kazachkov, B. Gong, B. Trouille, P. Donalek, Modeling Adjustable Speed Pumped Storage Hydro Units Employing Doubly-Fed Induction Machines, Tech. Rep. ANL/DIS-13/06, 2013 http://www.dis.anl.gov/psh.
[22] V. Koritarov, T.D. Veselka, J. Gasper, B.M. Bethke, A. Botterud, J. Wang, M. Mahalik, Z. Zhou, C. Milostan, J. Feltes, et al., Modeling and analysis of value of advanced pumped storage hydropower in the united states. http://www.osti.gov/scitech/biblio/1165600.
[23] V. Koritarov, L. Guzowski, J. Feltes, Y. Kazachkov, L. Baldwin, C. Grande-Moran, G. Thomann, L. Eng, B. Trouille, P. Donalek, Review of Existing Hydroelectric Turbine-Governor Simulation Models, Tech. Rep. ANL/DIS-13/05, 2013 http://www.dis.anl.gov/psh.
[24] J. Liang, R. Harley, Pumped storage hydro-plant models for system transient and long-term dynamic studies, in: IEEE Power and Energy Society General Meeting, 2010, pp. 1–8, http://dx.doi.org/10.1109/PES.2010.5589330.
[25] V. Azbe, R. Mihalic, Transient stability of a large doubly-fed induction machine in a pumped-storage plant, Electr. Power Syst. Res. 142 (2017) 29–35, http://dx.doi.org/10.1016/j.epsr.2016.08.043 https://www.sciencedirect.com/science/article/pii/S0378779616303479.
[26] S. Mansoor, D. Jones, D. Bradley, F. Aris, G. Jones, Stability of a pump storage hydro-power station connected to a power system, in: IEEE Power Engineering Society Winter Meeting, vol. 1, 1999, pp. 646–650, http://dx.doi.org/10.1109/PESW.1999.747531.
[27] H. Gao, C. Wang, A detailed pumped storage station model for power system analysis, in: IEEE Power Engineering Society General Meeting, 2006, pp. 5, http://dx.doi.org/10.1109/PES.2006.1709259.

[28] O. Nagura, M. Yoshida, Transient Behavior Analysis of Adjustable Speed Pumped Storage System, in: Hydro Vision International, 2011, pp. 414.
[29] T. Kuwabara, A. Shibuya, H. Furuta, E. Kita, K. Mitsuhashi, Design and dynamic response characteristics of 400 MW adjustable speed pumped storage unit for Ohkawachi Power Station, IEEE Trans. Energy Convers. 11 (2) (1996) 376–384, http://dx.doi.org/10.1109/60.507649.
[30] G. Osburn, P. Atwater, Design and testing of a back-to-back starting system for pumped storage hydrogenerators at Mt. Elbert Powerplant, IEEE Trans. Energy Convers. 7 (2) (1992) 280–288, http://dx.doi.org/10.1109/60.136222.
[31] Y. Pannatier, B. Kawkabani, C. Nicolet, J.-J. Simond, A. Schwery, P. Allenbach, Investigation of control strategies for variable-speed pump-turbine units by using a simplified model of the converters, IEEE Trans. Ind. Electron. 57 (9) (2010) 3039–3049 http://ieeexplore.ieee.org/xpls/abs_all.jsp?arnumber=5342518.
[32] T. Dal'Santo, A. Simões Costa, Hydroelectric unit commitment for power plants composed of distinct groups of generating units, Electr. Power Syst. Res. 137 (2016) 16–25, http://dx.doi.org/10.1016/j.epsr.2016.03.037 https://www.sciencedirect.com/science/article/pii/S0378779616300840.
[33] X. Guillaud, M.O. Faruque, A. Teninge, A.H. Hariri, L. Vanfretti, M. Paolone, V. Dinavahi, P. Mitra, G. Lauss, C. Dufour, et al., Applications of real-time simulation technologies in power and energy systems, IEEE Power Energy Technol. Syst. J. 2 (3) (2015) 103–115 http://ieeexplore.ieee.org/abstract/document/7234831/.
[34] M.O. Faruque, T. Strasser, G. Lauss, V. Jalili-Marandi, P. Forsyth, C. Dufour, V. Dinavahi, A. Monti, P. Kotsampopoulos, J.A. Martinez, et al., Real-time simulation technologies for power systems design, testing, and analysis, IEEE Power Energy Technol. Syst. J. 2 (2) (2015) 63–73 http://ieeexplore.ieee.org/abstract/document/7138557/.
[35] P. Forsyth, R. Kuffel, R. Wierckx, J.-B. Choo, Y.-B. Yoon, T.-K. Kim, Comparison of transient stability analysis and large-scale real time digital simulation, in: Power Tech Proceedings, 2001 IEEE Porto, vol. 4, IEEE, 2001, 7 pp. http://ieeexplore.ieee.org/abstract/document/964822/.
[36] A. Padoan, B. Kawkabani, A. Schwery, C. Ramirez, C. Nicolet, J.-J. Simond, F. Avellan, Dynamical behavior comparison between variable speed and synchronous machines with psS, IEEE Trans. Power Syst. 25 (3) (2010) 1555–1565, http://dx.doi.org/10.1109/TPWRS.2009.2039586.
[37] C. Nicolet, Hydroacoustic modelling and numerical simulation of unsteady operation of hydroelectric systems. http://infoscience.epfl.ch/record/98534.
[38] C. Nicolet, B. Greiveldinger, J.J. Hérou, B. Kawkabani, P. Allenbach, J.-J. Simond, F. Avellan, High-order modeling of hydraulic power plant in islanded power network, IEEE Trans. Power Syst. 22 (4) (2007) 1870–1880 http://ieeexplore.ieee.org/xpls/abs_all.jsp?arnumber=4349111.
[39] J. Koutnik, C. Nicolet, G.A. Schohl, F. Avellan, Overload surge event in a pumped-storage power plant, in: Proceedings of the 23rd IAHR Symposium on Hydraulic Machinery and Systems, 2006 http://infoscience.epfl.ch/record/104111.
[40] J.S. Czuba, L.N. Hannett, J.R. Willis, Implementation of power system stabilizer at the ludington pumped storage plant, IEEE Power Eng. Rev. PER-6 (2) (1986) 37–38, http://dx.doi.org/10.1109/MPER.1986.5528165 http://ieeexplore.ieee.org/lpdocs/epic03/wrapper.htm?arnumber=5528165.
[41] T. Ackermann, Wind Power in Power Systems, Wiley, 2005 https://books.google.com/books?id=f7MDGCiOgiMC.
[42] E. Muljadi, M. Singh, V. Gevorgian, M. Mohanpurkar, R. Hovsapian, V. Koritarov, Dynamic modeling of adjustable-speed pumped storage hydropower plant, in: IEEE Power Engineering Society General Meeting, 2015, Denver, CO, 2015.
[43] R. Oldenburg, J. Donelson, Dynamic response of a hydroelectric plant, AIEE Trans. (1962) 403–419.
[44] R. Allan, M.R.G. Al-Shakarchi, Probabilistic techniques in a.c. load-flow analysis, Proc. Inst. Electr. Eng. 124 (2) (1977) 154–160, http://dx.doi.org/10.1049/piee.1977.0027.
[45] X. Guan, P. Luh, H. Yen, P. Rogan, Optimization-based scheduling of hydrothermal power systems with pumped-storage units, IEEE Trans. Power Syst. 9 (2) (1994) 1023–1031, http://dx.doi.org/10.1109/59.317641.